

Improved entanglement entropy estimates from filtered bitstring probabilities

Avi Kaufman, James Corona, Zane Ozzello, Muhammad Asaduzzaman, and Yannick Meurice
Department of Physics and Astronomy, The University of Iowa, Iowa City, IA 52242, USA

(Dated: January 7, 2025)

Using the bitstring probabilities of ground states of bipartitioned ladders of Rydberg atoms, we calculate the mutual information which is a lower bound on the corresponding bipartite von Neumann quantum entanglement entropy S_A^{vN} . We show that in many cases, these lower bounds can be improved by removing the bitstrings with a probability lower than some value p_{min} and renormalizing the remaining probabilities (filtering). Surprisingly, in some cases, as we increase p_{min} the filtered mutual information tends to plateaus at values very close to S_A^{vN} over some range of p_{min} . We consider various sizes, lattice spacings and bipartitions. Our numerical investigation suggest that the filtered mutual information obtained with samples having just a few thousand bitstrings can provide reasonably close estimates of S_A^{vN} . We briefly discuss practical implementations with the QuEra’s Aquila device.

Introduction. Recent progress in the controlled manipulation of small quantum systems has opened the possibility of using quantum devices to study aspects of lattice models considered in condensed matter or high energy physics which cannot be obtained efficiently with classical computing [1, 2]. In this context, arrays of Rydberg atoms have been used to build quantum simulators for lattice gauge theory models [3–12]. A specific example of quantum simulator is a ladder of Rydberg atoms. Initially designed to simulate scalar QED [7], it does not provide an exact match to the target model [13]. However it has a very rich phase diagram that includes Berezinskii–Kosterlitz–Thouless transition, Conformal Field Theory critical points and incommensurate (floating) phases [14, 15]. This offers multiple opportunities to define continuum limits in regions of parameter space where the correlation lengths are large compared to the lattice spacing. Exploring large parameter spaces to identify the critical regions requires efficient methods.

An important quantity to study phase transitions and the critical behavior is the entanglement entropy [16–32]. The experimental measurement of entanglement entropy is challenging due to its nonlocal nature. One possibility is to prepare and interfere copies of the original system [30–37]. This is experimentally feasible, however it remains labor consuming and not the ideal tool for extensive phase space exploration. Recently it was empirically observed [38] that for arrays of Rydberg atoms, the classical mutual information I_{AB}^X for a bipartition AB obtained from the easily accessible bitstring distributions of a single copy, provides lower bounds that are observed to be rather close to S_A^{vN} . For the quantum von Neumann entropy $S_A^{vN} = S_B^{vN}$. The lower bound property

$$I_{AB}^X \leq S_B^{vN} = S_A^{vN}, \quad (1)$$

follows from Holevo bound [38–40].

In this work we show that this bound can be improved by “filtering” or “truncating” the bitstring probabilities, which means removing the measurements which occur less than a given number of times and renormalizing the kept measurements. This can be achieved by ignoring measurements of states $|\{n\}\rangle$ such that the fraction of

observations $N_{\{n\}}/N_{shots} \leq p_{min}$. In the supplementary material of [38], it was observed that when the ramping down of the Rabi frequency before measurement was too slow, large probabilities were amplified and small probabilities reduced. This has resemblance to the filtering described above. It was then shown that for samples of 1000 bitstrings, removing the states with less than 10 observations ($p_{min} = 0.01$), increased I_{AB}^X in 6 out of 7 examples considered. In the following, we discuss systematically the effect of p_{min} on the mutual information $I_{AB}^X(p_{min})$. To our surprise, it was found that in some cases, the increase in mutual information was followed by plateaus where $I_{AB}^X(p_{min}) \simeq S_A^{vN}$. A particularly convincing illustration is shown in Fig. 1. The dashed line represents an accurate value of I_{AB}^X without filtering. Almost no changes occur for $p_{min} \leq 10^{-4}$, then, as we increase p_{min} up to 10^{-2} , $I_{AB}^X(p_{min})$ transitions from the unfiltered value to values close to S_A^{vN} .

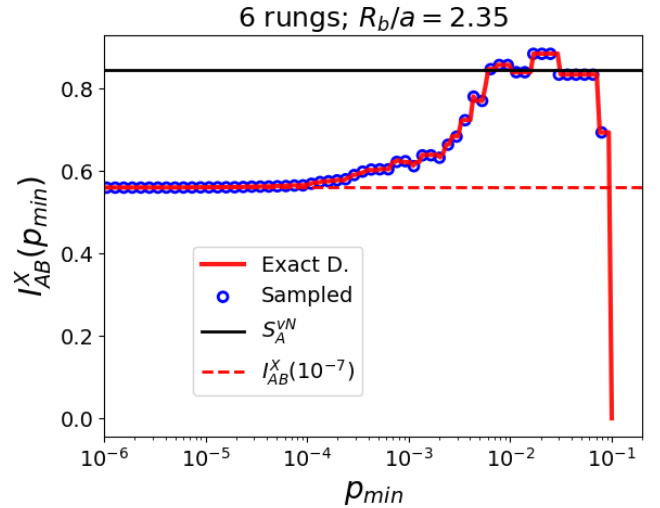


FIG. 1: $I_{AB}^X(p_{min})$ for a six-rung ladder with exact diagonalization (continuous line) and DMRG sampling (open circles). Details are provided in Appendix A.

In the following, we introduce the specific model used

for calculations, a ladder of Rydberg atoms, and perform calculations with exact diagonalization, DMRG methods and, remote operation of the Aquila facilities. We discuss the dependence of the truncated mutual information on the size of the system, the lattice spacing, and the bipartition of the system. This provides a more nuanced picture than the specific example of Fig. 1. Our conclusions involve a discussion of the consequences for experiments with limited resources, typically a few thousands shots.

The simulator: ladder of Rydberg atoms. Recently, it has become possible to create arrays of Rydberg atoms with adjustable geometries [41–46]. Their Hamiltonian reads

$$H = \frac{\Omega}{2} \sum_i (|g_i\rangle \langle r_i| + |r_i\rangle \langle g_i|) - \Delta \sum_i \hat{n}_i + \sum_{i < j} V_{ij} \hat{n}_i \hat{n}_j, \quad (2)$$

with van der Waals interactions $V_{ij} = \Omega R_b^6 / r_{ij}^6$, for a distance r_{ij} between the atoms labelled as i and j . We use $\hbar = 1$ units. We follow the convention of using a characteristic length scale, blockade radius R_b , at which if two Rubidium atoms are placed, the interaction strength V_{ij} equals to the Rabi frequency Ω . We define the Rydberg occupation $\hat{n}_i |r_i\rangle = |r_i\rangle$ while $\hat{n}_i |g_i\rangle = 0$. In the following, we focus on a two leg ladder where the rung length a_y is twice the distance between rungs a_x , which is also the lattice spacing denoted a hereafter. This is illustrated in Fig. 2. This choice is motivated by the rich critical behavior observed in Ref. [14] especially for $R_b/a \simeq 2.35$ for sufficiently large volume. However, we used open boundary condition for a rectangular shape rather than shifted boundary conditions in [14]. We conducted numerical calculations using density matrix renormalization group (DMRG) [47] and remote analog quantum simulations using the QuEra’s Aquila device [48] which is publicly available. Details are provided in the Appendix. B.

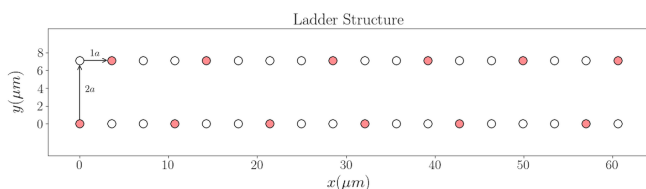


FIG. 2: Illustration of the lattice structure for an 18 rung ladder with ground state (empty circle) and Rydberg state (red circle) atoms.

Bipartite setup. For a Rydberg array with N_q atoms either in the ground $|g\rangle$ or Rydberg $|r\rangle$ the whole system (AB) can be divided in two subsystems A and B . The computational basis consists of the 2^{N_q} elements

$$|\{n\}\rangle \equiv |n_0, n_1, \dots, n_{N_q-1}\rangle, \quad (3)$$

with $n_j = 0$ or 1 representing $|g\rangle$ and $|r\rangle$ respectively. Note that some authors use the opposite convention. Any

element of this basis can be factored in a bi-partite way by splitting the N_q qubits into $|A\rangle$ and $|B\rangle$ qubits with $|A| + |B| = N_q$.

$$|\{n\}_{AB}\rangle = |\{n\}_A\rangle |\{n\}_B\rangle, \quad (4)$$

with

$$|\{n\}_A\rangle \equiv |n_0, n_1, \dots, n_{|A|-1}\rangle \text{ and} \quad (5)$$

$$|\{n\}_B\rangle \equiv |n_{|A|}, \dots, n_{N_q-1}\rangle \quad (6)$$

Given an arbitrary prepared state $|\psi\rangle$, we can write it as a superposition of the states in the computational basis

$$|\psi\rangle = \sum_{\{n\}} c_{\{n\}} |\{n\}\rangle. \quad (7)$$

Using $\rho_{AB} = |\psi\rangle \langle \psi|$, the reduced density matrix of the subsystem A is defined as $\rho_A = \text{Tr}_B(\rho_{AB})$ and the corresponding von Neumann entanglement entropy

$$S_A^{vN} = -\text{Tr}(\rho_A \ln(\rho_A)) = -\sum_m \lambda_m \ln(\lambda_m), \quad (8)$$

where λ_m ’s are the eigenvalues of ρ_A which are independent of the basis used in A . In an experiment, the state $|\{n\}\rangle$ is observed with a probability

$$p_{\{n\}} = |c_{\{n\}}|^2. \quad (9)$$

We define the associated Shannon entropy as

$$S_{AB}^X \equiv -\sum_{\{n\}} p_{\{n\}} \ln(p_{\{n\}}), \quad (10)$$

Following Shannon [49] we define the marginal probability in the subsystem A by summing over B :

$$p_{\{n\}_A} = \sum_{\{n\}_B} p_{\{n\}_A \{n\}_B}, \quad (11)$$

and the corresponding entropy

$$S_A^X \equiv -\sum_{\{n\}_A} p_{\{n\}_A} \ln(p_{\{n\}_A}). \quad (12)$$

Similarly, we can define S_B^X by interchanging A and B in the above equations. The classical mutual information is defined as

$$I_{AB}^X \equiv S_A^X + S_B^X - S_{AB}^X. \quad (13)$$

It was found by Shannon [49] that this quantity is non-negative. Upper bounds can also be found by reducing ρ_A to the diagonal part ρ_A^X [50, 51]. In summary [38–40] we have the bounds:

$$0 \leq I_{AB}^X \leq S_B^{vN} = S_A^{vN} \leq S_A^X \text{ (or } S_B^X). \quad (14)$$

Illustrations of the behavior of these quantities as functions of the adjustable parameters are given in Appendix

C in the case of a six-rung ladder. The numerical methods used to calculate the vacuum state and sample the probabilities are presented in Appendix D. The errors associated with the finite size of the sampling are illustrated in Appendix E.

Effects of the filtration on S_A^{vN} . It should be noted that in Fig.1, the truncated mutual information gets slightly larger than S_A^{vN} which seems to conflict with the bound in Eq. (1). For instance, $I_{AB}^X(0.01) \simeq 0.857 > S_A^{vN} \simeq 0.844$. However, it should be remembered that the truncated probability distribution is the diagonal part of the truncated density matrix. Calculating S_A^{vN} for the density matrix obtained with the truncated ground state (see below), we obtain $S_A^{vN}(0.01) \simeq 1.132$ which is consistent with the bound.

In general we can introduce a projector corresponding to a given filtration

$$P(p_{min}) = \sum_{\{n\}: p_{\{n\}} \geq p_{min}} |\{n\}\rangle \langle \{n\}|. \quad (15)$$

Given a state $|\psi\rangle$, we define the normalized projected state as

$$|\psi, p_{min}\rangle = P(p_{min}) |\psi\rangle / \sqrt{\langle \psi | P(p_{min}) | \psi \rangle} \quad (16)$$

and the corresponding density matrix and entropies. We then have the bound

$$I_{AB}^X(p_{min}) \leq S_B^{vN}(p_{min}) = S_A^{vN}(p_{min}). \quad (17)$$

As shown in Fig. 3 this bound is clearly obeyed. Moreover, the distance between the bound and the target value stays more or less constant ($\simeq 0.3$).

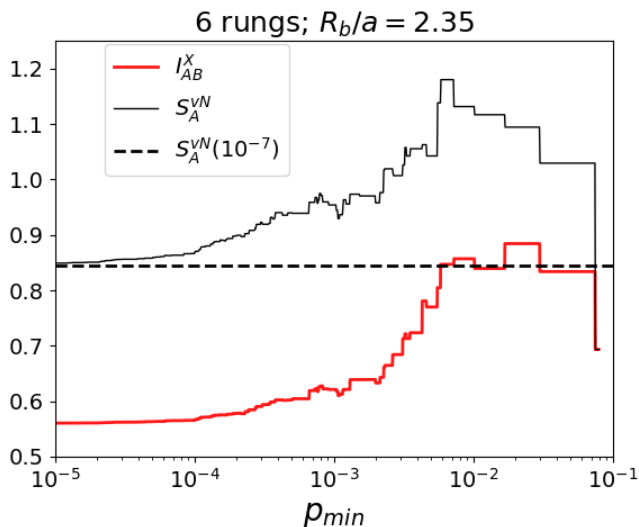


FIG. 3: $I_{AB}^X(p_{min})$ and $S_A^{vN}(p_{min})$ for a six-rung ladder with exact diagonalization.

Where should we stop? Since the filtered mutual information is not necessarily a lower bound of the unfiltered S_A^{vN} , we need to determine the optimal value of

p_{min} . Fig. 1 suggests that we could stop when I_{AB}^X stops increasing over a “significant” range. Note that there are short range fluctuations due to the discrete nature of the probabilities which are clearly seen on Fig. 3. Consequently the non-increasing property should be seen for scales larger than the fluctuations.

Volume dependence. We repeated the procedure described for Fig. 1 but with more rungs. The results are shown in Fig. 4. We see that up to 18 rungs, if we terminate the truncation process when the mutual information stops growing we obtain better estimates of S_A^{vN} than the untruncated ones. For 20 rungs, $I_{AB}^X(p_{min})$ decreases over a large part of the left side and this suggests to pick the untruncated value which empirically appears to be a rather tight lower bound. For 22 rungs, the first obvious peak overshoots the exact S_A^{vN} by an amount comparable to the error for the untruncated lower bound. There are some short plateaus which may be considered as more conservative choices.

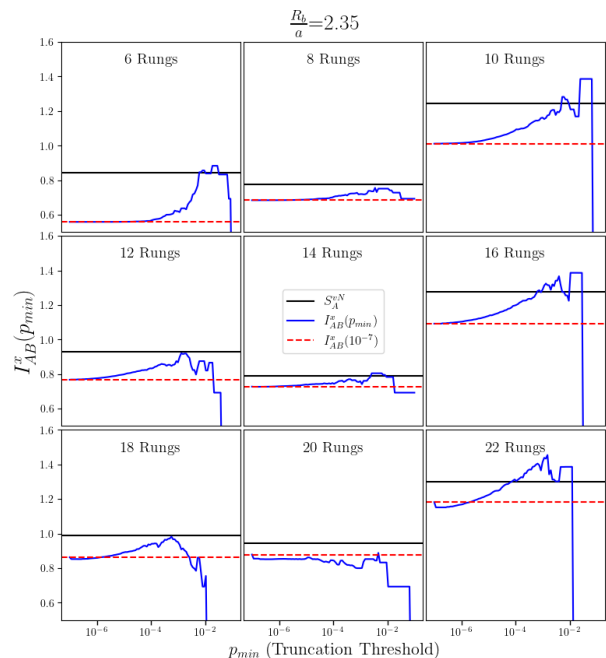


FIG. 4: Effects of the system size on $I_{AB}^X(p_{min})$ for 6, 8, ..., 22 rungs, $R_b/a = 2.35$ and 10 million counts obtained via DMRG.

Lattice spacing dependence. We have considered the effect of changing the lattice spacing on $I_{AB}^X(p_{min})$. For $R_b/a = 1.00$, the entanglement is very low and so is $I_{AB}^X(p_{min})$ over a broad range on the left. For R_b/a between 1.25 and 2.25, there are some significant plateaus at values between the untruncated I_{AB}^X and S_A^{vN} . For R_b/a between 2.5 and 3.00, there are in addition broader plateaus at values very slightly above S_A^{vN} . Again some judgment is required.

Bipartition dependence. This method of estimating entanglement entropy is not limited to just bipartitions

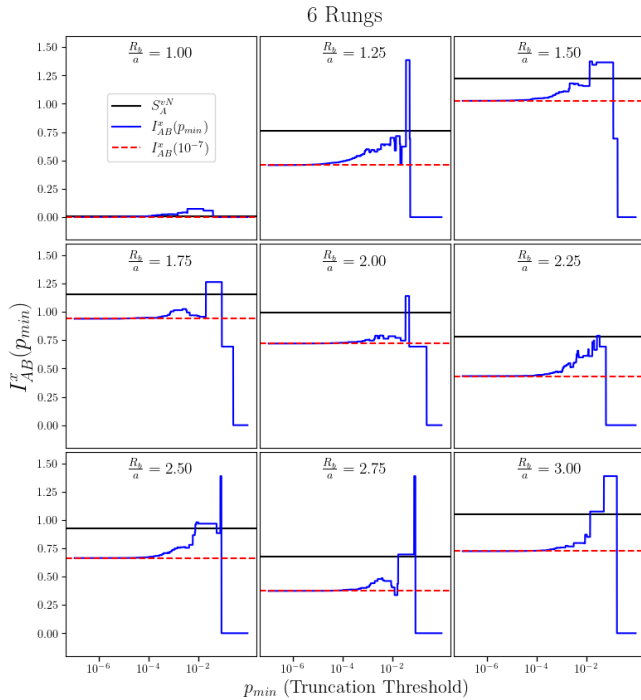


FIG. 5: Effects of the lattice spacing on $I_{AB}^X(p_{min})$ for $R_b/a = 1.0, 1.25, \dots, 3.0$, 6 rungs and 10 million counts obtained via DMRG.

with $|A| = |B|$. This is shown in Fig. 6 where a Rydberg ladder of 8 rungs and $R_b/a = 2.35$ is investigated. The methodology is just the same as before, using Eq. (13), but now the sizes $|A|$ and $|B|$ need not be equal. The von Neumann entropy and the mutual information are both symmetric under the interchange of A and B and subsystems with $|A| = 2$ and 14 , 4 and 12 , etc. provide identical results. When incorporating the filtered probabilities with varying subsystems it is observed that the filtration reaches closer to the von Neumann entropy when the von Neumann entropy is lower. This behavior is shown in Fig. 6 where we also see that a value $p_{min} \sim 10^{-2}$ is close to the best improvement for all subsystem sizes of this volume.

Analog simulations with Aquila. So far we relied on numerical methods to obtain vacuum states and their associated probabilities. In this subsection, we discuss results obtained by adiabatically preparing the vacuum states and then performing measurements using Quera’s Aquila Rydberg atom device. See Appendix B for more information. As a first step, we considered the case of 6 rungs with $R_b/a = 2.35$ and compared with the exact results of Fig. 1. We performed several experiments of 1000 shots each and performed a comparison of the variation in shot counts for the computation of filtered mutual information. It is clear from the comparison with the exact diagonalization results in Fig. 7, that increasing the number of shots from 1000 to 4000 tends to improve the filtered mutual information $I_{AB}^X(p_{min})$. How-

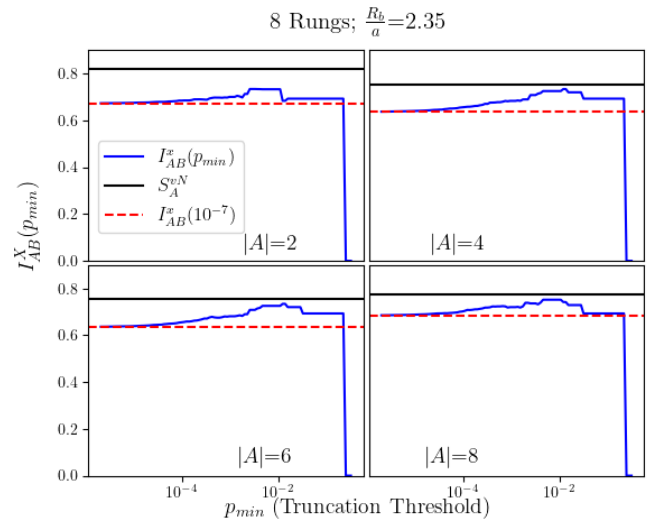


FIG. 6: Illustration of the effects of truncation for differing subsystem sizes for a bipartition. This behavior mirrors for equivalent sizing. Probabilities obtained with 10 million counts of DMRG.

ever, aside from the statistical error, there are several sources of experimental errors including waveform error, detection error, scattering from the intermediate state due to lasers [45]. In some cases the discrepancies with numerical results are significant and cannot be understood as statistical errors. The sources of these errors and potential mitigation strategies are currently under investigation. More results obtained from Aquila, with other lattice spacings and number of rungs are provided in Appendix F.

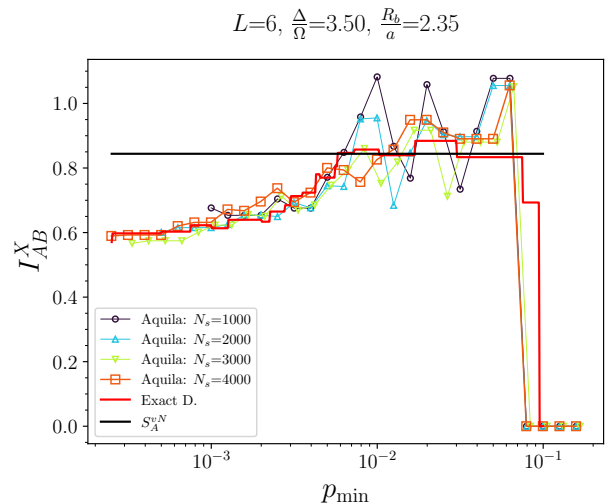


FIG. 7: The number of shots is varied to investigate the deviation of the Aquila simulation result with the exact diagonalization.

Estimates of S_A^{vN} with a few thousands shots. In our numerical calculations, we were able to have either all the probabilities using exact diagonalization, or millions of shots distributed in good approximation as in the exact results when using the DMRG. However, as far as improving the mutual information bound, the states with low probabilities don't play an important role. Typically, we observe significant onsets near $p_{min} \sim 10^{-4}$ which suggests that we can get improved estimations of S_A^{vN} using only a few thousand shots. This is illustrated in the example of Fig. 7, where we approximately reproduce the exact filtered mutual information $I_{AB}(p_{min})$ with $p_{min} \geq 10^{-3}$. This is good news, because when using actual physical quantum devices, one is often limited to extract information from a few thousands shots.

As additional illustrations, we have collected $I_{AB}(10^{-3})$ for $R_b/a = 2.35$ with different numbers of rungs with even bipartitions and 12 rungs for various bipartitions (Fig. 8). In all but two cases, this simple procedure provides values above the unfiltered mutual information and below the target value. These two figures rely on DMRG calculations with 10^7 shots where states with a probability 10^{-3} appear approximately 10,000 times. On the other hand, if we have only 3,000 shots, the same states are expected to appear 3 times and the error on the estimated probability is much larger. Fig. 8 shows that for the examples considered here, the choice $p_{min} = 10^{-3}$ tends to provide significant, but not necessarily optimal, improvements allowing estimation of the quantum entanglement with limited resources.

Conclusions. Using examples of ladders of Rydberg atoms, we have shown that by excluding bitstrings with probabilities lower than p_{min} and renormalizing the remaining data, a procedure that we call filtering, we tend to obtain larger mutual information and better approximations to the von Neumann entanglement entropy S_A^{vN} . As the filtered mutual information does not in general provide a lower bound on S_A^{vN} , the optimal value for p_{min} requires some discussion. A conservative approach would be to stop when the mutual information stops increasing over a range of p_{min} which is large compared to the range for small fluctuations due to the discrete nature of the probabilities. Current efforts are underway to automatize the selection of an improved filtration level to achieve a filtered level closer to the true von Neumann value with an emphasis being placed around the areas of relative plateau as potential such bounds.

In a significant number of cases considered, we found consistent plateaus where the filtered mutual information closely approximates S_A^{vN} over a broad range of values. The reasons for this behavior are not well understood. The existence of plateaus simply signals that there are gaps in the distributions of probabilities. What is surprising is that they often coincide with the approach of the target value for S_a^{vN} . It maybe tempting to speculate that the low probability states are "featureless" as far as the diagonal part of the the density matrix is concerned, and that removing them provides a better estimate of

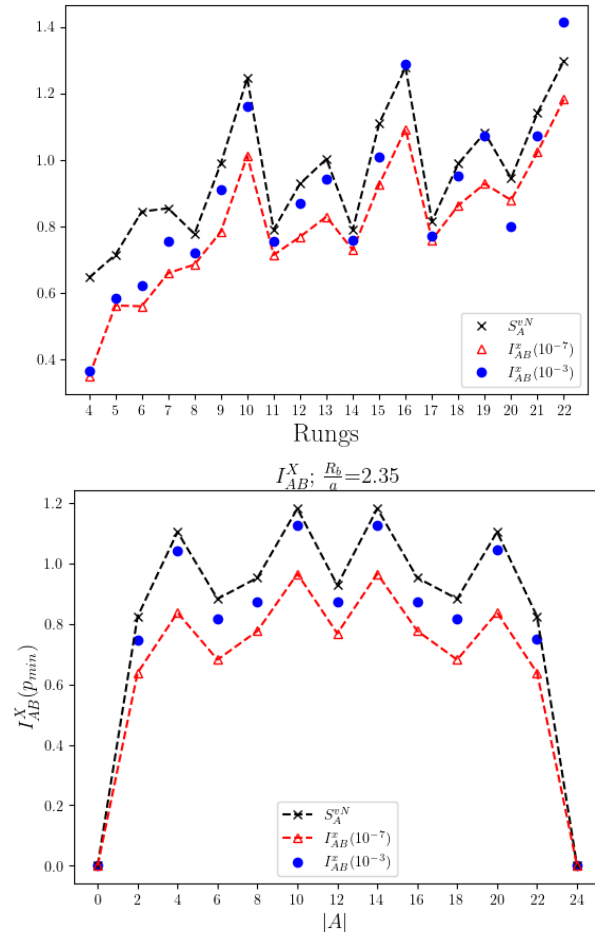


FIG. 8: $I_{AB}(10^{-7})$ (triangles), $I_{AB}(10^{-3})$ (filled circles) and S_A^{vN} (crosses) for $R_b/a = 2.35$ and 10 million shots obtained via DMRG. Top: for 4, 5, ..., 22 rungs with even bipartitions; Bottom: for 12 rungs with different bipartitions.

the quantum entanglement. However, as shown in Fig. 3, the removal of these states affects the quantum entanglement and the idea needs to be refined. It should also be mentioned that sometimes the plateaus are replaced by peaks.

Analog simulations with a few thousands shots provide a limited access to states with low probabilities and naturally provide significantly filtered data. The origin of the discrepancies between Aquila data and numerical methods is currently under investigation. More specifically, we are characterizing errors due to imperfect state preparation, Ω ramping down, readout errors and statistical errors. Future work may extend these techniques to larger systems and more complex geometries, furthering their applications for analog simulations.

Acknowledgements. This research was supported in part by the Dept. of Energy under Award Number

DE-SC0019139. We thank the Amazon Web Services and S. Hassinger for facilitating remote access to QuEra through the Amazon Braket while teaching quantum mechanics and our Department of Physics and Astronomy for supporting part of the cost of the analog simulations presented here. We thank the University of Iowa for providing access to the Argon computing facilities. We acknowledge the use of NERSC facilities with ERCAP 0023235 award. We thank B. Senseman for helpful comments. Discussions during the long-term workshop, HHIQCD2024, at Yukawa Institute for Theoretical Physics (YITP-T-24-02), were useful as we completed this work.

Appendix A: Detailed features of Fig. 1

In this Appendix, we discuss specific aspects of Fig. 1 in the main text. We calculated the vacuum of a 6 rung ladder with $R_b/a=2.35$. This first choice of lattice spacing was motivated by the rich critical behavior found in Ref. [14]. We first used exact diagonalization and extracted an accurate value for $S_A^{vN} \simeq 0.844$ (top horizontal line in Fig.1) for A being the 3 rungs on say the left side of the ladder. We then calculated the probabilities to observe any of the 4096 states available in the computational basis and obtained the mutual information $I_{AB}^X \simeq 0.559$ which is about 30 percent below S_A^{vN} (dashed line). We then removed the states with a probability less than p_{min} , starting with $p_{min} = 10^{-6}$, renormalized the remaining probabilities and then recalculated the filtered $I_{AB}^X(p_{min})$.

We then repeated the vacuum calculation using MPS and the DMRG method to generate 10^7 random states with probabilities corresponding to the $|c_n|^2$ using a recursive method available with ITensor (see Appendix D). This can be thought to be an ideal experiment with 10^7 shots. The results are in excellent agreement with the exact diagonalization which validates the DMRG method that will be used for larger volumes when exact diagonalization becomes difficult.

Appendix B: Quantum device simulation methods

We conducted remote analog quantum simulations using QuEra’s Aquila device [48]. The motivation behind this is to investigate larger system sizes which at some point will become inaccessible with classical computation methods. With the naive exact diagonalization we could investigate a Rydberg system of size $N_q = 12$ atoms, whereas with high-precision DMRG calculation we could investigate up to a system size $N_q = 44$ atoms. In the near future, we will be able to investigate models with far more atoms than this with the quantum device. Aquila has a roadmap for extending their device to simulate more than 3000 atoms by 2025 [53].

We prepared the ground state of the system adiabatically. Initially we prepare a state with all the atoms in the ground state. Incidentally, this is the ground state of the Rydberg system at infinite negative detuning and zero Rabi frequency. Next, we slowly tune the Rabi frequency from zero to the target frequency (Ω) and in the same duration, we increase the detuning from a large negative value to the target value (Δ). Ideally due to the slow adiabatic evolution we can reach the ground state of the target parameters as the system is gapped. In experiments, before any measurement is performed, Rabi frequency is switched off as this is essential for the fluorescence imaging in the readout process [41]. This is done as fast as possible so that the ground state of the target Hamiltonian is minimally disrupted by other low lying energy states. There are different choices on how to tune the parameters in the Rydberg simulation to prepare ground state at different phases. Once we set the lattice spacing a to a fixed number, we can set the final Rabi frequency and final detuning to different values to recover the ground state at different phases. For the Aquila simulation, we use the same parameters to that of DMRG simulation in all the cases, except for the case $R_b/a = 3.0$, where we use $\Omega = 0.4982\pi$ MHz due to the geometrical constraint that distance between two nearest neighbor atoms needs to be less than $4 \mu\text{m}$ at the current publicly available setup at Aquila device.

Appendix C: Phase diagram and bound on entanglement entropy

In this appendix, we present the entanglement entropy for a six-rung ladder as a function of R_b/a and Δ/Ω . The results are shown in Fig. 9. For small systems, the results are sensitive to the system size and boundary conditions. For a detailed overview on different phases in the Rydberg ladder at larger volumes and different boundary conditions see [14].

In Fig. 10, we plotted the bitstring entropy S_{AB}^X , the reduced bitstring entropy S_A^X , the von Neumann entropy S_A^{vN} and the classical mutual information I_{AB}^X as we vary the inverse lattice spacing in blockade-radius unit. We observe agreement with the rigorous bounds $0 \leq I_{AB}^X \leq S_A^{vN} \leq S_A^X$. We also observe that S_A^{vN} becomes larger when the gap closes.

Appendix D: Numerical methods

Numerical calculations were performed with $\Omega = 5\pi$ MHz, which implies $R_b = 8.375\mu\text{m}$, and a detuning $\Delta = 17.5\pi$ MHz as in [14]. R_b/a was varied between 1 and 3. Exact diagonalization calculations were performed in python using the linalg library. The DMRG calculations of vacua and the samples of measurements with the corresponding probability were performed with the ITensor software library in Julia [52].

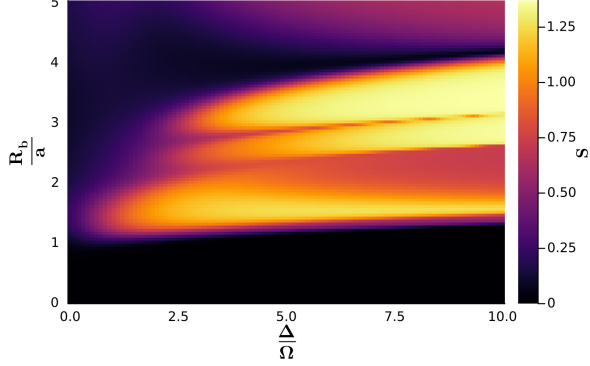


FIG. 9: von Neumann entanglement entropy for a six-rung ladder with $a_y = 2a_x$ as a function of R_b/a_x and Δ/Ω .

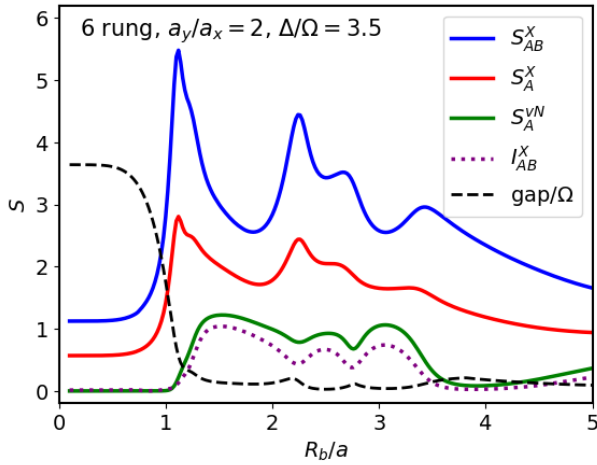


FIG. 10: Comparison of S_{AB}^X , S_A^X , S_A^{vN} and I_{AB}^X at a fixed $\Delta/\Omega = 3.5$.

Appendix E: Fluctuations in finite sampling

With the current technology, the number of shots obtained in analog simulations is much lower than the 10 million shots obtained with the DMRG. Using QuEra’s Aquilla device [48] we are able to produce 1000 shots on a consistent basis. In order to produce DMRG data that resembles experimental output, we randomly reduce our sample size to 1000 shots. To see the impact a smaller sample size has on the error of the mutual information, we do this smaller sample size 1000 times. From these 1000 samples of 1000 shots we calculate error bars. Fig. 11 shows the high accuracy DMRG (10 million shots) plotted against the Sampled DMRG (1000 shots) with error bars. The figure shows that the randomly selected DMRG subsamples roughly follow the shape of the higher accuracy DMRG. This puts the analog calculation discrepancies in perspective.

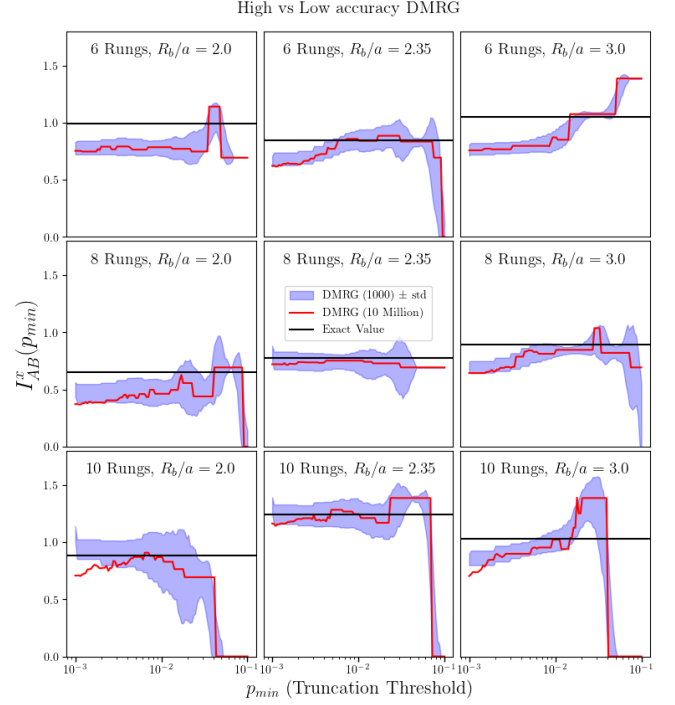


FIG. 11: DMRG (10 million counts) vs DMRG (1000 shots with error) for various R_b/a and system sizes.

Appendix F: Other analog simulations

We performed analog quantum simulations with Aquila for three different sizes of the ladder and at three different R_b/a at a fixed $\Delta/\Omega = 3.5$. The results are shown in Fig. 12. We observe that some of the qualitative features of the filtered classical mutual information are consistent with the DMRG computation. In some cases, we observe an increase in the filtered mutual information as we increase p_{min} . However, the position of the peak in the filtered entropy doesn’t always coincide with the DMRG computation. The discrepancy is smaller for the shorter ladders. Since the process of filtering probabilities involves characterizing all states including low probability states, and the Hilbert space grows exponentially with the number of atoms ($\dim(H) \propto 2^{N_q}$), recovering quantitative result for the filtered mutual information become challenging with low statistics. A quantitative analysis of the statistical requirements on the volume warrants further study. We also note a larger discrepancy as the ratio of R_b/a is increased, this is predominantly due to the larger errors associated in the laser waveforms for cases with higher ratio. A detailed study of this issue is currently being investigated and authors will present the results elsewhere.

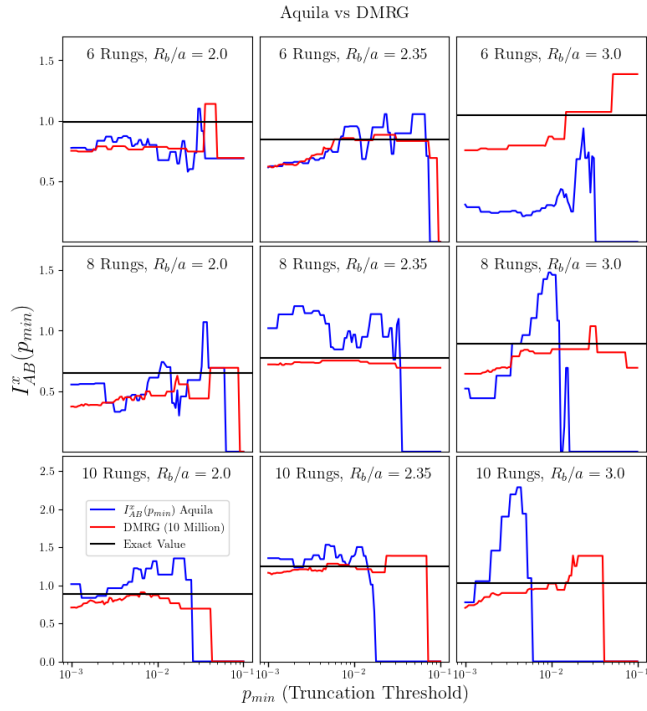


FIG. 12: Filtered mutual information obtained from DMRG (10^7 samples of ground states) vs Aquilla (2000 shots) for various Rb/a (2.0, 2.35 and 3.0) and system sizes (6, 8 and 10 rungs).

-
- [1] Christian W. Bauer et al., “Quantum Simulation for High-Energy Physics,” *PRX Quantum* **4**, 027001 (2023), arXiv:2204.03381 [quant-ph].
- [2] Ehud Altman et al., “Quantum Simulators: Architectures and Opportunities,” *PRX Quantum* **2**, 017003 (2021), arXiv:1912.06938 [quant-ph].
- [3] Jin Zhang, J. Unmuth-Yockey, J. Zeiher, A. Bazavov, S.-W. Tsai, and Y. Meurice, “Quantum simulation of the universal features of the polyakov loop,” *Phys. Rev. Lett.* **121**, 223201 (2018).
- [4] Federica M. Surace, Paolo P. Mazza, Giuliano Giudici, Alessio Lerose, Andrea Gambassi, and Marcello Dalmonte, “Lattice gauge theories and string dynamics in rydberg atom quantum simulators,” *Phys. Rev. X* **10**, 021041 (2020).
- [5] Simone Notarnicola, Mario Collura, and Simone Montangero, “Real-time-dynamics quantum simulation of $(1 + 1)$ -dimensional lattice qed with rydberg atoms,” *Phys. Rev. Res.* **2**, 013288 (2020).
- [6] Alessio Celi, Benoît Vermersch, Oscar Viyuela, Hannes Pichler, Mikhail D. Lukin, and Peter Zoller, “Emerging Two-Dimensional Gauge Theories in Rydberg Configurable Arrays,” *Phys. Rev. X* **10**, 021057 (2020), arXiv:1907.03311 [quant-ph].
- [7] Yannick Meurice, “Theoretical methods to design and test quantum simulators for the compact Abelian Higgs model,” *Phys. Rev. D* **104**, 094513 (2021), arXiv:2107.11366 [quant-ph].
- [8] Pierre Fromholz, Mikheil Tsitsishvili, Matteo Votto, Marcello Dalmonte, Alexander Nersisyan, and Titas Chanda, “Phase diagram of rydberg-dressed atoms on two-leg triangular ladders,” *Phys. Rev. B* **106**, 155411 (2022).
- [9] Daniel González-Cuadra, Torsten V. Zache, Jose Carrasco, Barbara Kraus, and Peter Zoller, “Hardware Efficient Quantum Simulation of Non-Abelian Gauge Theories with Qudits on Rydberg Platforms,” *Phys. Rev. Lett.* **129**, 160501 (2022), arXiv:2203.15541 [quant-ph].
- [10] Kenneth Heitritter, Yannick Meurice, and Stephen Mrenna, “Prolegomena to a hybrid Classical/Rydberg simulator for hadronization (QuPYTH),” (2022), arXiv:2212.02476 [quant-ph].
- [11] Jad C. Halimeh, Monika Aidelsburger, Fabian Grusdt, Philipp Hauke, and Bing Yang, “Cold-atom quantum simulators of gauge theories,” (2023), arXiv:2310.12201 [cond-mat.quant-gas].
- [12] Daniel Gonzalez-Cuadra et al., “Observation of string breaking on a $(2 + 1)$ D Rydberg quantum simulator,” (2024), arXiv:2410.16558 [quant-ph].
- [13] Jin Zhang, S. W. Tsai, and Y. Meurice, “Critical behavior of lattice gauge theory Rydberg simulators from effective Hamiltonians,” *Phys. Rev. D* **110**, 034513 (2024), arXiv:2312.04436 [quant-ph].
- [14] Jin Zhang, Sergio H. Cantú, Fangli Liu, Alexei Bylinskii, Boris Braverman, Florian Huber, Jesse Amato-Grill, Alexander Lukin, Nathan Gemelke, Alexander Keesling, Sheng-Tao Wang, Y. Meurice, and S. W. Tsai, “Probing quantum floating phases in rydberg atom arrays,” (2024), arXiv:2401.08087 [quant-ph].
- [15] Shu-Ao Liao, Jin Zhang, and Li-Ping Yang, “Phase diagram of Rydberg atoms in a two-leg rectangular ladder,” (2024), arXiv:2412.11201 [cond-mat.quant-gas].
- [16] Luigi Amico, Rosario Fazio, Andreas Osterloh, and Vlatko Vedral, “Entanglement in many-body systems,” *Reviews of Modern Physics* **80**, 517 (2008).
- [17] J. Eisert, M. Cramer, and M. B. Plenio, “Area laws for the entanglement entropy - a review,” *Rev. Mod. Phys.* **82**, 277–306 (2010), arXiv:0808.3773 [quant-ph].
- [18] Shinsei Ryu and Tadashi Takayanagi, “Holographic derivation of entanglement entropy from AdS/CFT,” *Phys. Rev. Lett.* **96**, 181602 (2006), arXiv:hep-th/0603001.
- [19] Dmitry A. Abanin, Ehud Altman, Immanuel Bloch, and Maksym Serbyn, “Colloquium : Many-body localization, thermalization, and entanglement,” *Reviews of Modern Physics* **91** (2019), 10.1103/revmodphys.91.021001.
- [20] J. Ignacio Cirac, David Perez-Garcia, Norbert Schuch, and Frank Verstraete, “Matrix product states and projected entangled pair states: Concepts, symmetries, theorems,” *Rev. Mod. Phys.* **93**, 045003 (2021), arXiv:2011.12127 [quant-ph].
- [21] Sudip Ghosh, Ronak M Soni, and Sandip P. Trivedi, “On The Entanglement Entropy For Gauge Theories,” *JHEP* **09**, 069 (2015), arXiv:1501.02593 [hep-th].
- [22] Karel Van Acoleyen, Nick Bultinck, Jutho Haegeman, Michael Marien, Volkher B. Scholz, and Frank Verstraete, “The entanglement of distillation for gauge theories,” *Phys. Rev. Lett.* **117**, 131602 (2016), arXiv:1511.04369 [quant-ph].
- [23] Mari Carmen Bañuls, Krzysztof Cichy, J. Ignacio Cirac, Karl Jansen, and Stefan Kühn, “Efficient basis formulation for $1+1$ dimensional $SU(2)$ lattice gauge theory: Spectral calculations with matrix product states,” *Phys. Rev. X* **7**, 041046 (2017), arXiv:1707.06434 [hep-lat].
- [24] Johannes Knaute, Matan Feuerstein, and Erez Zohar, “Entanglement and confinement in lattice gauge theory tensor networks,” *JHEP* **02**, 174 (2024), arXiv:2401.01930 [quant-ph].
- [25] Dmitri E. Kharzeev and Eugene M. Levin, “Deep inelastic scattering as a probe of entanglement,” *Phys. Rev. D* **95**, 114008 (2017), arXiv:1702.03489 [hep-ph].
- [26] O. K. Baker and D. E. Kharzeev, “Thermal radiation and entanglement in proton-proton collisions at energies available at the cern large hadron collider,” *Phys. Rev. D* **98**, 054007 (2018).
- [27] Kun Zhang, Kun Hao, Dmitri Kharzeev, and Vladimir Korepin, “Entanglement entropy production in deep inelastic scattering,” *Phys. Rev. D* **105**, 014002 (2022), arXiv:2110.04881 [quant-ph].
- [28] Silas R. Beane, David B. Kaplan, Natalie Klco, and Martin J. Savage, “Entanglement Suppression and Emergent Symmetries of Strong Interactions,” *Phys. Rev. Lett.* **122**, 102001 (2019), arXiv:1812.03138 [nucl-th].
- [29] Caroline Robin, Martin J. Savage, and Nathalie Pillet, “Entanglement Rearrangement in Self-Consistent Nuclear Structure Calculations,” *Phys. Rev. C* **103**, 034325 (2021), arXiv:2007.09157 [nucl-th].
- [30] G. Vidal, J. I. Latorre, E. Rico, and A. Kitaev, “Entanglement in quantum critical phenomena,” *Phys. Rev. Lett.* **90**, 227902 (2003).
- [31] V. E. Korepin, “Universality of entropy scaling in one dimensional gapless models,” *Phys. Rev. Lett.* **92**, 096402

- (2004).
- [32] Pasquale Calabrese and John L. Cardy, “Entanglement entropy and quantum field theory: A Non-technical introduction,” *Int. J. Quant. Inf.* **4**, 429 (2006), arXiv:quant-ph/0505193.
- [33] Dmitry A. Abanin and Eugene Demler, “Measuring entanglement entropy of a generic many-body system with a quantum switch,” *Phys. Rev. Lett.* **109**, 020504 (2012).
- [34] A. J. Daley, H. Pichler, J. Schachenmayer, and P. Zoller, “Measuring entanglement growth in quench dynamics of bosons in an optical lattice,” *Phys. Rev. Lett.* **109**, 020505 (2012).
- [35] Rajibul Islam, Ruichao Ma, Philipp M. Preiss, M. Eric Tai, Alexander Lukin, Matthew Rispoli, and Markus Greiner, “Measuring entanglement entropy in a quantum many-body system,” *Nature* **528**, 77–83 (2015).
- [36] Adam M. Kaufman, M. Eric Tai, Alexander Lukin, Matthew Rispoli, Robert Schittko, Philipp M. Preiss, and Markus Greiner, “Quantum thermalization through entanglement in an isolated many-body system,” *Science* **353**, 794–800 (2016).
- [37] J. Unmuth-Yockey, Jin Zhang, P. M. Preiss, Li-Ping Yang, S. W. Tsai, and Y. Meurice, “Probing the conformal Calabrese-Cardy scaling with cold atoms,” *Phys. Rev. A* **96**, 023603 (2017), arXiv:1611.05016 [cond-mat.quant-gas].
- [38] Yannick Meurice, “Experimental lower bounds on entanglement entropy without twin copy,” (2024), arXiv:2404.09935 [quant-ph].
- [39] John Preskill and Mehdi Soleimanifar, “Private communication,” (2024).
- [40] Tai-Hsuan Yang, Mehdi Soleimanifar, Thiago Bergamaschi, and John Preskill, “When can classical neural networks represent quantum states?” (2024), arXiv:2410.23152 [quant-ph].
- [41] Hannes Bernien, Sylvain Schwartz, Alexander Keesling, Harry Levine, Ahmed Omran, Hannes Pichler, Soonwon Choi, Alexander S. Zibrov, Manuel Endres, Markus Greiner, Vladan Vuletić, and Mikhail D. Lukin, “Probing many-body dynamics on a 51-atom quantum simulator,” *Nature* **551**, 579–584 (2017).
- [42] Alexander Keesling, Ahmed Omran, Harry Levine, Hannes Bernien, Hannes Pichler, Soonwon Choi, Rhine Samajdar, Sylvain Schwartz, Pietro Silvi, Subir Sachdev, Peter Zoller, Manuel Endres, Markus Greiner, Vladan Vuletić, and Mikhail D. Lukin, “Quantum kibble-zurek mechanism and critical dynamics on a programmable rydberg simulator,” *Nature* **568**, 207–211 (2019).
- [43] Henning Labuhn, Daniel Barredo, Sylvain Ravets, Sylvain de Léséleuc, Tommaso Macrì, Thierry Lahaye, and Antoine Browaeys, “Tunable two-dimensional arrays of single rydberg atoms for realizing quantum ising models,” *Nature* **534**, 667–670 (2016).
- [44] Sylvain de Léséleuc, Vincent Lienhard, Pascal Scholl, Daniel Barredo, Sebastian Weber, Nicolai Lang, Hans Peter Büchler, Thierry Lahaye, and Antoine Browaeys, “Observation of a symmetry-protected topological phase of interacting bosons with rydberg atoms,” *Science* **365**, 775–780 (2019).
- [45] Sepehr Ebadi, Tout T. Wang, Harry Levine, Alexander Keesling, Giulia Semeghini, Ahmed Omran, Dolev Bluvstein, Rhine Samajdar, Hannes Pichler, Wen Wei Ho, Soonwon Choi, Subir Sachdev, Markus Greiner, Vladan Vuletić, and Mikhail D. Lukin, “Quantum phases of matter on a 256-atom programmable quantum simulator,” *Nature* **595**, 227–232 (2021).
- [46] Pascal Scholl, Michael Schuler, Hannah J. Williams, Alexander A. Eberharter, Daniel Barredo, Kai-Niklas Schymik, Vincent Lienhard, Louis-Paul Henry, Thomas C. Lang, Thierry Lahaye, Andreas M. Läuchli, and Antoine Browaeys, “Quantum simulation of 2d antiferromagnets with hundreds of rydberg atoms,” *Nature* **595**, 233–238 (2021).
- [47] Ulrich Schollwöck, “The density-matrix renormalization group,” *Reviews of modern physics* **77**, 259–315 (2005).
- [48] Jonathan Wurtz, Alexei Bylinskii, Boris Braverman, Jesse Amato-Grill, Sergio H. Cantu, Florian Huber, Alexander Lukin, Fangli Liu, Phillip Weinberg, John Long, Sheng-Tao Wang, Nathan Gemelke, and Alexander Keesling, “Aquila: Quera’s 256-qubit neutral-atom quantum computer,” (2023), arXiv:2306.11727 [quant-ph].
- [49] C.E. Shannon and W. Weaver, *The Mathematical Theory of Communication*, Illini books (University of Illinois Press, 1949).
- [50] John Preskill, “Quantum information chapter 10: quantum Shannon theory,” (2022).
- [51] Edward Witten, “A Mini-Introduction To Information Theory,” *Riv. Nuovo Cim.* **43**, 187–227 (2020), arXiv:1805.11965 [hep-th].
- [52] Matthew Fishman, Steven R. White, and E. Miles Stoudenmire, “The ITensor Software Library for Tensor Network Calculations,” *SciPost Phys. Codebases*, 4 (2022).
- [53] “Quera computing releases a groundbreaking roadmap for advanced error-corrected quantum computers, pioneering the next frontier in quantum innovation,” (2024), accessed: 2024-11-05.